Integrative Biology

PAPER

Cite this: *Integr. Biol.*, 2014, 6, 946

Exploitation of the hepatic stellate cell Raman signature for their detection in native tissue samples

Kerstin Galler,[ab] Franziska Schleser,[bc] Esther Fröhlich,[bc] Robert Pascal Requardt,[b] Andreas Kortgen,[bc] Michael Bauer,[bc] Jürgen Popp[abde] and Ute Neugebauer*[ab]

Received 5th June 2014,
Accepted 11th August 2014

DOI: 10.1039/c4ib00130c

www.rsc.org/ibiology

Hepatic stellate cells (HSCs) surround liver sinusoids and store retinol while they are quiescent. During fibrotic liver diseases and acute-on-chronic liver failure they change to the activated state in which they proliferate, lose their retinol content and deposit extracellular matrix molecules. The process of HSC activation is of utmost interest, but so far only insufficiently understood, because there is a lack of techniques to address the function of single HSCs in the tissue context. In this contribution, the potential of Raman micro-spectroscopy for the label-free detection of HSCs in mouse liver samples is demonstrated. First, culture-induced activation of primary mouse HSCs is followed *in vitro* and characterized by means of Raman spectroscopy. The HSC activation state is confirmed by immunofluorescence labeling of glial fibrillary acidic protein (GFAP) and α-smooth muscle actin (ASMA). As expected, the unique Raman spectrum of retinol in quiescent HSCs is lost during activation. Nevertheless, successful discrimination of HSCs from primary hepatocytes is possible during all states of activation. A classification model based on principal component analysis followed by linear discriminant analysis (PCA–LDA) of the lipid droplet Raman data yields a prediction accuracy of 99%. The *in vitro* results are transferred to fresh liver slices and freshly sampled livers. Quiescent HSCs and a HSC transforming from quiescent to activated state are identified based on their Raman signature. This provides valuable information on HSC activation state in the liver.

Insight, innovation, integration

HSC activation is critical for acute and chronic liver diseases. Label-free identification of this specific cell type at different levels of activation in freshly sampled, unprocessed liver based on its vibrational spectroscopic signature is shown. Raman micro-spectroscopy as a non-destructive technique was employed to characterize HSC Raman features *in vitro*. No external labels were required and living material could be used. The specific Raman signatures served as basis for HSC detection on single cell level in the whole mouse liver *ex vivo*. This approach allows for the assessment of living samples without harming it with energy-rich UV light necessary for HSC detection using retinol autofluorescence. In addition, a tentative conclusion on HSC activation state is permitted from the Raman data.

Introduction

Hepatic stellate cells (HSCs) are specialized liver cells storing about 80% of a mammal's retinol in their quiescent state. They are pericytes that surround small liver vessels called sinusoids. Thus, the stellate cells constitute a connection between the most abundant liver cell type, the hepatocyte, and endothelial cells lining sinusoid walls (Fig. 1A).[1] They also contribute in immune reactions.[2] However, HSCs receive special interest as key players in acute-on-chronic liver failure caused by portal hypertension[3,4] and in the chronic process of liver fibrosis.[5,6] Furthermore, they may be involved in hepatocarcinogenesis.[6–8] In disease onset and propagation HSCs change their phenotype remarkably. They adopt a stretched, fibroblast-like shape and gain positivity for α-smooth muscle actin (ASMA),[9,10] a well-established myofibroblast marker.[11–13] Furthermore, the retinol content of HSCs decreases during activation.[10,14] HSCs produce large amounts of extracellular matrix molecules which they deposit in their surroundings. By this they contribute to

[a] *Leibniz Institute of Photonic Technology, Jena, Germany. E-mail: ute.neugebauer@med.uni-jena.de*
[b] *Center for Sepsis Control and Care, Jena University Hospital, Germany*
[c] *Department of Anesthesiology and Intensive Care Medicine, Jena University Hospital, Germany*
[d] *Institute of Physical Chemistry and Abbe Center of Photonics, Friedrich Schiller University Jena, Germany*
[e] *InfectoGnostics Forschungscampus Jena, Zentrum für Angewandte Forschung, Jena, Germany*

This journal is © The Royal Society of Chemistry 2014

Downloaded from https://academic.oup.com/ib/article/6/10/946/5199050 by University of Alabama at Birmingham user on 27 May 2022

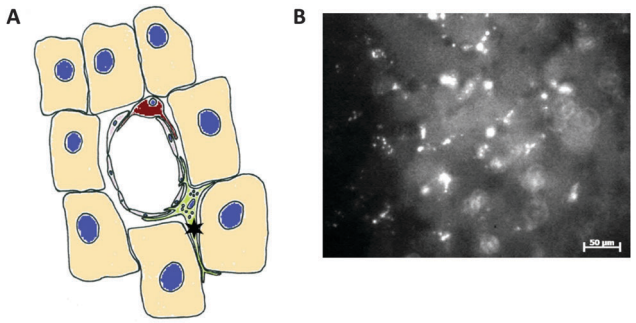

Fig. 1 HSCs in tissue. (A) Scheme of the liver tissue structure. A sinusoide lined by fenestrated endothelium is surrounded by hepatocytes and non-parenchymal cells. The HSC (labeled by a star) is positioned in the space of Disse. (B) Retinol autofluorescence (λ_{ex} = 365 nm) on the surface of fresh liver represented by light dots.

scar formation.[15] Thus, a detailed understanding of the HSC activation process is of high interest for deeper insights into the progression of fibrosis. Such knowledge is the prerequisite for the development of strategies against progression of fibrosis and associated diseases.[14,16] However, as current technologies cannot follow HSC activation *in vivo* without the destruction of the cell at selected time points or the insertion of an external label, such as a fluorophore, the HSC activation process is still only incompletely understood. While resting HSCs can be identified by their retinol autofluorescence (Fig. 1B), identification of activated HSCs requires insertion of a fluorescent label which can have an influence on cell features and behavior. *Via* genetic engineering fluorescent proteins like green fluorescent protein (GFP) and its derivatives can be introduced. However, those molecules are large (GFP consists of 238 amino acids[17]). To avoid GFP induced artifacts labeling after experiments is possible, but can only be performed at dead matter. For the quiescent and activated state of *in vitro* cultured HSCs expression profiles on mRNA and to some extend on protein level are available.[10,18,19] Efforts were made to reveal molecular activation mediators[20–22] and retinoid metabolism.[14,23,24] Yet, further insights will require careful cell interaction studies and the tracking of activation in living cells. This sets an urgent need for a label-free cell identification method that has the potential to be applied *in vivo* as well.

Raman spectroscopy, a vibrational spectroscopic method that relies on inherent molecular properties, could be such a solution. Monochromatic laser light is used to excite the Raman scattering. In contrast to fluorescence excitation no specific excitation wavelength is needed to cause the Raman effect. Therefore, experimental conditions can be chosen so that laser induced damage on the sensitive living biological sample can be prevented. This involves optimization with respect to laser wavelength, laser power and sample exposure time.[25,26] Raman spectroscopy has been successfully adapted to study biological material within the last twenty years[27–29] and now enables spectroscopic discrimination of different cell types, such as healthy and cancerous cells[30,31] or lymphocyte sub-populations.[32] Drug-induced changes in the chemical composition of tumor cells were analyzed[33] and tumor tissue grading is possible.[34,35] In addition, advanced Raman spectroscopy is capable of documenting deep layer tissue composition.[36] Raman spectroscopic imaging combined with sophisticated data processing allows for the visualization of different cellular compartments.[37] It was applied to follow cytochrome *c* dynamics during apoptosis in a completely label-free manner.[38] Furthermore, phenotypic changes accompanying *in vitro* culture of chondrocytes[39] as well as hepatocyte[40] were addressed and changes in HSC lipid droplets were studied.[41]

In this contribution, primary hepatocytes and HSCs are characterized during the *in vitro* activation process. Both cell types can be discriminated against each other based on their Raman data during all stages of HSC activation even at the point, when HSCs have already lost all retinol content. In addition, HSCs can be localized in fresh mouse whole liver samples and living slices based on their Raman spectroscopic signature. Areas with HSC Raman pattern in the spectra are clearly delineatable against the surrounding. This spectroscopic detection causes minimal tissue damage and does not rely on any external label. Therefore, this method is perfectly suited for further studies of the activation process in physiologic tissue surrounding.

Results and discussion

Label-free characterization of culture-induced activation of primary HSCs

HSCs have been isolated from mouse livers of healthy animals and cultured for up to 14 days to induce activation. Raman spectroscopy was used to follow and spectroscopically characterize the culture-induced activation, *i.e.*, the change from the quiescent state at day 0 to the activated state at day 14. As Raman spectroscopy does not alter the cells, *in vitro* activation was confirmed after the Raman measurements by immunofluorescence staining. The HSC quiescence marker glial fibrillary acidic protein (GFAP)[10,42] and the activation marker α-smooth muscle actin (ASMA)[9,10] served to fulfill this need (Fig. 2A).

The freshly isolated cells at day 0 were embedded in alginate to allow Raman spectroscopic imaging; at later time points cells had adhered to the substrate. Laser light of 532 nm wavelength was chosen for vibrational excitation to obtain images with high spatial resolution. Furthermore, this wavelength is in pre-resonance to the $\pi\pi^*$ transition of retinol, thus, yielding intense vibrational retinol bands due to the pre-resonance Raman effect. N-FINDR analysis was utilized to generate false color Raman images revealing cellular compartments such as nucleus and droplets filled with retinol and/or lipids (Fig. 2B). Averaged Raman spectra of those compartments are shown in Fig. 3. Raman spectra of biological matter share some degree of similarity caused by the common overall chemical composition. The Raman spectra of nuclei (Fig. 3A), *e.g.*, all reflect typical vibrational features of nucleic acids such as the PO_2^- vibration at about 1092 cm^{-1} or the spectral features at 786 cm^{-1} and 1372 cm^{-1} assignable to the nucleic acid bases. In addition, prominent CH vibrational contributions at 1450 cm^{-1} and 2935 cm^{-1} as well as features which indicate proteins are visible at 1002 cm^{-1}, 1254 cm^{-1} and

Downloaded from https://academic.oup.com/ib/article/6/10/946/5199050 by University of Alabama at Birmingham user on 27 May 2022

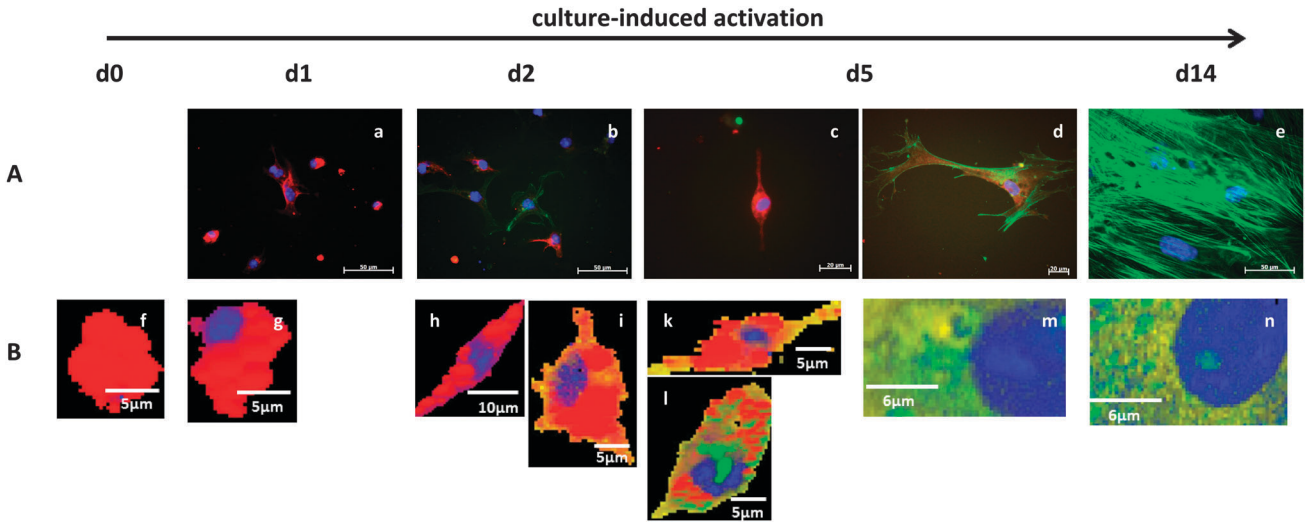

Fig. 2 HSC phenotype transition during culture-induced activation. Images from *in vitro* cultured HSCs reflect the ongoing spreading of the cells with cultivation time. (A) In the fluorescence images (a–e) a change in the expression of GFAP (red) and ASMA (green) is visible accompanying prolonged *in vitro* culture. Nuclei are visible from DAPI fluorescence (blue). Scale bars in (a), (b), (e) indicate 50 µm, scale bars in c and d indicate 20 µm. (B) Representative N-FINDR false-color Raman images (f–n) show the cellular compartments: nucleus (blue), lipid droplets containing retinol (red), lipid droplets without retinol (green), and cytoplasm (yellow). Notably, the intracellular space occupied by retinol decreases with ongoing activation and vanishes completely in fully activated HSCs at d5 and d14 after isolation.

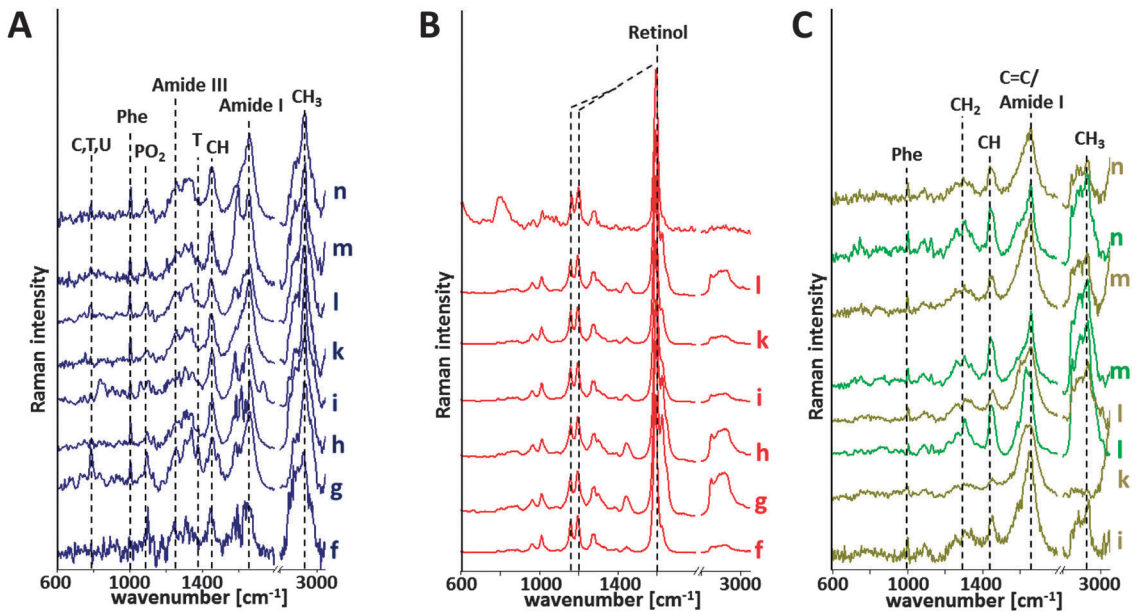

Fig. 3 Average Raman spectra of the N-FINDR Raman images presented in Fig. 2B. The spectra reflect intra- and intercellular chemical differences. (A) Nuclei spectra contain vibrational contributions from PO_2^- and nucleic acid bases. (B) Retinoid spectra detected inside the cells resemble the retinyl palmitate reference spectrum depicted on top. (C) Remaining spectra show features from lipid and proteins.

1657 cm^{-1} in those spectra.[43,44] The latter are present in the cytoplasm spectra depicted in Fig. 3C as well. Cellular components with a different chemical structure, such as retinol with its five double bonds in a polyene chain, yield a unique Raman scattering pattern. The Raman spectrum of a retinyl palmitate solution in isopropanol raises an especially sharp and intense peak at 1593 cm^{-1} (Fig. 3B, top spectrum) due to the C=C stretching vibration.[45] This vibrational signature is also found in the quiescent HSCs (Fig. 2B, f–l and 3B) which are known to store retinol in esterificated form.[1] Therefore, the retinol Raman signal can be used as a valuable intrinsic marker of resting HSCs.

Raman spectra of HSCs directly after isolation (day 0) are dominated by the characteristic retinol vibrational signature. Often, the cells were nearly entirely filled with retinol as shown in the false color Raman maps (Fig. 2B, f). With prolonged *in vitro* cultivation, a gradual decrease in the cellular retinol content was

Downloaded from https://academic.oup.com/ib/article/6/10/946/5199050 by University of Alabama at Birmingham user on 27 May 2022

 This journal is © The Royal Society of Chemistry 2014

observed as can be seen in the representative Raman images in Fig. 2B. At day 1 after isolation when cells had attached to the substrates, they were still loaded with retinol as is concluded from the Raman data (Fig. 2B, g). At that time point all HSCs were positive for GFAP, while ASMA fluorescence was completely absent indicating the resting state of the freshly isolated HSCs (Fig. 2A, a). During the following days, cells gained ASMA positivity while they lost GFAP expression. However, this process was not concerted for all cells, *i.e.* at day 5 after isolation some HSCs were still in the quiescent state (Fig. 2A, c and B, k) while others were already activated (Fig. 2A, d and B, m). The culture-induced activation was accompanied by a drastic decrease in retinol content (Fig. 2 and 4). At the end of observation at day 14, cells had stretched remarkably and showed overwhelming ASMA fluorescence after staining. GFAP positivity had vanished completely (Fig. 2A, e). Dramatic cell enlargement and development of a layer like structure (confluence) prevented complete cell Raman maps at day 14. Retinol was never detected in cultured HSCs at that time point; instead lipid droplets without retinol were then present (Fig. 2B, n and 3C, n). These results connect the change from expression of GFAP to the activation marker ASMA with the presence of retinol in HSCs on a single cell level. The Raman data are gained after minimal sample preparation in a label-free way and show excellent agreement with literature data on the retinol loss during activation obtained by traditional biochemical bulk analysis[14,21] as well as on the expression of HSC markers derived by time and resource consuming methods, such as polymerase chain reaction (PCR), Western blot and immunofluorescence.[10,16,46]

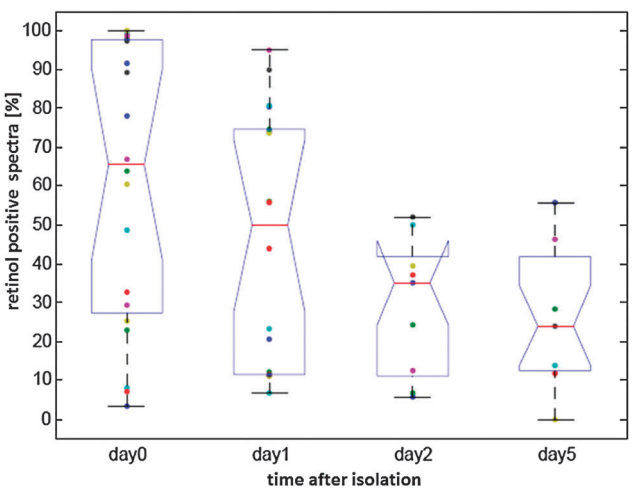

Fig. 4 Decrease in HSC retinol content accompanying prolonged cultivation calculated from relative retinol content in the N-FINDR false color Raman images for the first 5 days. At day 14 retinol was never found in the HSCs. Spectra were counted as retinol positive if the retinol endmember contributed with at least 75%. Each dot in the boxplot represents the retinol content of an individual HSC, red horizontal lines represent the median retinol content in the cells per day. Median differences between days are significant if notches do not overlap. Top and bottom of each box represent the 25th and 75th percentile of the data, respectively. Whiskers extend 1.5 times the interquartile range.

In this study, the specific Raman spectroscopic fingerprint of HSCs at different activation states was identified (Fig. 2B and 3). The retinol content decreases upon activation and other lipid droplets without retinol are present in the activated stellate cells. A detailed analysis of the lipid spectra of the activated HSCs is beyond the scope of this manuscript. However, the Raman spectroscopic signature of the retinol-free lipid droplets in HSCs indicates the presence of unsaturated fatty acid species. This is in good agreement with Testerink *et al.* who used high-performance liquid chromatography, mass spectrometry (HPLC-MS) and Raman spectroscopic studies to reveal the replacement of retinol by polyunsaturated fatty acids.[41] Compared to Testerink *et al.* our study extends also to the day of isolation (day 0) where we could find HSCs that are almost completely occupied by retinol containing lipid droplets (Fig. 2B, f). In disagreement with the results from Testerink *et al.*,[41] the substitution process does not always seem to be homogenous for all lipid droplets of a certain cell. Fig. 2B, l shows a Raman image of a hepatic stellate cell containing retinol filled lipid droplets as well as other lipid droplets containing no retinol, but other lipid species instead. Nevertheless, it is emphasized that this was only a rare finding concerning three out of 16 measured cells at day 2 and 5 after isolation.

Distinguishing HSCs and hepatocytes based on their Raman data

The ultimate goal is to identify hepatic stellate cells in the liver in a label-free manner. Therefore, a Raman spectroscopy-based algorithm has to be developed to distinguish HSCs from hepatocytes. Hepatocytes are the most common cell type in the liver which makes up to 80% of the cell mass in the liver.[47] As was done for HSCs, hepatocytes were isolated from mouse livers and false color Raman images from *in vitro* cultured cells were generated employing the N-FINDR algorithm. Lipid droplets, nucleus and cytoplasm can be revealed in the Raman maps (Fig. 5A). Morphological features are reflected, *e.g.*, occasional polyploidy of hepatocytes (Fig. 5A and B).

Average Raman spectra for each cell compartment (lipid droplet, nucleus, cytochrome rich cytoplasm) were calculated from single spectra that contribute to the respective N-FINDR endmember with at least 75% and are depicted in Fig. 5C. The vibrational features of the hepatocyte nuclei are very similar to the ones of HSCs (Fig. 3A) showing, *e.g.*, PO_2^- and nucleic acid base vibrations at 1092 cm^{-1} and 784 cm^{-1}, respectively.

Typical vibrational features which are only found in HSCs are the retinol patterns which, however, get lost upon activation (Fig. 2B, 3B and 4). Therefore, they are only useful to identify quiescent stellate cells. Significant differences can also be found when comparing the vibrational bands of the remaining retinol-free lipid droplets in the activated HSCs and those of the lipid droplets in hepatocytes. Especially the intensity ratio of the vibrational bands of the C=C stretching vibration at 1650 cm^{-1} and the CH deformation at 1440 cm^{-1} differs remarkably between lipid droplets of both cell types. The ratio of these Raman peak intensities can be used to deduce fatty acid saturation as was introduced by Davies and Hodge.[48]

Downloaded from https://academic.oup.com/ib/article/6/10/946/5199050 by University of Alabama at Birmingham user on 27 May 2022

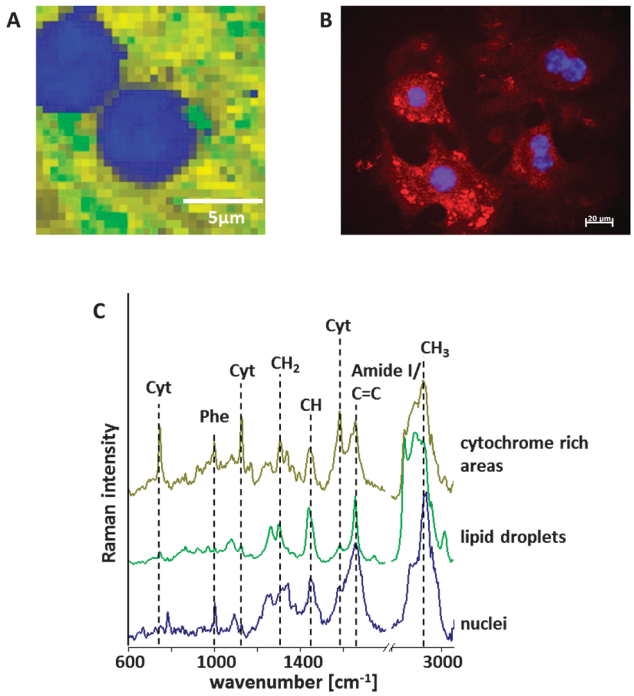

Fig. 5 Hepatocytes. (A) Representative N-FINDR false color Raman image and (B) fluorescence image. (C) Average Raman spectra for the cell compartments visible in A: nuclei (blue), lipid droplets (green) and cytochrome (Cyt) rich areas (yellow). In the fluorescence image nuclei are visible *via* DAPI fluorescence (blue), the epithelial marker E-cadherin is shown in red.

For HSC lipid droplets this ratio reflects a certainly higher degree of unsaturation than for hepatocyte lipid droplets.

Hepatocytes show in part of their cytoplasm region sharp vibrational bands at 748 cm^{-1}, 1128 cm^{-1} and 1587 cm^{-1} (Fig. 5C). These bands can be assigned to vibrational contributions of cytochromes.[49,50] The presence of high amounts of cytochromes in hepatocytes is well established since those hemoproteins play a major role during detoxification of xenobiotics.[51]

To estimate the possibility of HSC identification in mixed cell populations or tissue environment, unsupervised statistical analysis was carried out to discriminate isolated HSCs and hepatocytes *via* principal component analysis (PCA). As cells display very different Raman spectra in their different compartments, individual analysis was carried out: (1) using lipid droplet spectra (without retinol) and (2) using nuclei spectra. N-FINDR analysis of the individual Raman cell maps was employed to assign single spectra to the respective compartment (lipid droplet and nucleus, respectively). Only single spectra contributing to a compartment specific N-FINDR endmember with at least 75% (lipid droplets) and 80% (nuclei) were included for further analysis. The resulting PCA score plots are shown in Fig. 6A (lipid droplets) and Fig. 6C (nuclei). A good separation between HSCs and hepatocytes was achieved when using spectra derived from lipid droplets (Fig. 6A). The first principal component (PC1) carries most of the information necessary for separation. However, it cannot be used alone to correctly distinguish all hepatocytes from HSC. The continuous streaking of individual data points belonging to HSC lipid droplets in the PCA plot (Fig. 6A) can be explained by a varying contribution of lipid vibrations to the individual spectra, especially the C=C vibration at 1650 cm^{-1} and the CH vibration around 1440 cm^{-1}, as those spectral features are also reflected in the PC1 loading (Fig. 6B). This corresponds to a varying lipid concentration inside the cell. The single spectra are acquired next to each other in a single cell. Thus, when scanning over a larger lipid droplet, a continuous increase and decrease in the lipid amount in the laser focus is observed. In general, the loadings (Fig. 6B) show that important lipid features at 1650 cm^{-1}, 1440 cm^{-1} and 1266 cm^{-1} contribute to the separation. This is in excellent agreement with the visible differences in lipid droplet average spectra described above. It is important to emphasize that this reliable differentiation was carried out with retinol-free HSC lipid droplets. This means, Raman-based differentiation of hepatocytes and HSCs is also possible when HSCs have been maintained in prolonged culture and thus have adopted the activated phenotype.

The best result for unsupervised nuclei differentiation could be obtained using PC2 and PC3 (Fig. 6C). However, the loadings (Fig. 6D) contain a lot of noise with a few features at 1660 cm^{-1}, 1585 cm^{-1}, 1452 cm^{-1} and 793 cm^{-1}. The resulting differentiation of hepatocytes and HSCs is not as clear as when using the lipid spectra. Thus, in the following only lipid spectra of hepatocytes and HSCs were used for supervised statistical analysis.

A PCA–linear discriminant analysis (PCA–LDA) classification model for the cell type differentiation was built using 250 spectra of non-retinol containing HSC lipid droplets and 182 spectra of hepatocyte lipid droplets. Within this training data set no misclassification was observed (Table 1A). The model was tested with an independent data set containing 518 spectra derived from HSCs and hepatocytes from an independent isolation process from a different animal resulting in an overall identification accuracy of 99% (Table 1B). The LDA loading with prominent features in the regions of the C=C stretching vibration[43] (around 1642 cm^{-1}) and the CH deformation vibration[43] (around 1266 cm^{-1}) (Fig. 6E) reflects the importance of the spectroscopic contributions from lipids for successful differentiation. Therefore, in the following *in situ* studies, lipid vibrational contributions receive special attention.

Raman-based imaging and cell type assignment in living tissue slices

Thin precision-cut living tissue slices are an ideal model to access and study cells in more physiologic surrounding than the traditional cell culture environment. Organ architecture is maintained keeping the cells in their natural niche and in close contact with each other as well as with the extracellular matrix. Metabolism is close to the *in vivo* situation.[52,53] However, due to the tightness of the cell collective, cell type identities are hard to define but of utmost interest for elucidation of inter-cellular interactions.

Raman spectroscopic imaging was applied to such thin precision-cut liver slices. In order to minimize potential photodamage, the Raman excitation wavelength was shifted to the NIR (785 nm). Fig. 7A shows a false color Raman image of such

Downloaded from https://academic.oup.com/ib/article/6/10/946/5199050 by University of Alabama at Birmingham user on 27 May 2022

 This journal is © The Royal Society of Chemistry 2014

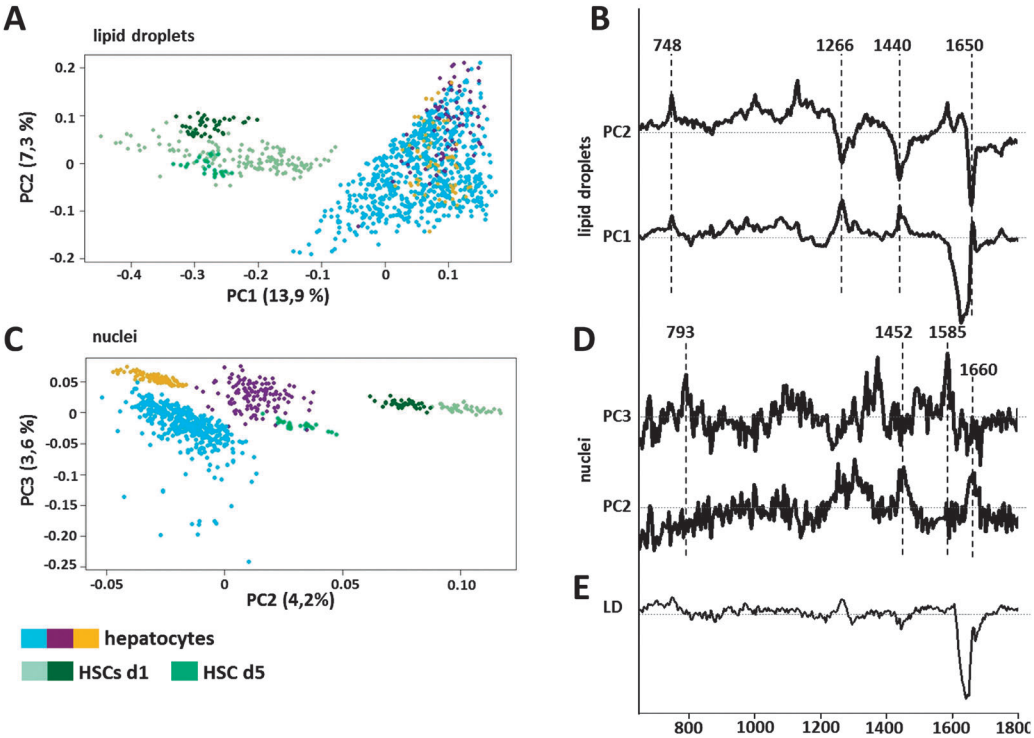

Fig. 6 Differentiation of HSCs and hepatocytes. (A and C) PCA score plots with Raman spectra from three different HSCs (green) and three different hepatocytes (blue, violet, orange). (A) Each dot represents a Raman spectrum from a lipid droplet (without retinol) and (C) a Raman spectrum from the nucleus. (B and D) PCA loadings corresponding to (A) and (C), respectively. (E) LDA loading corresponding to the PCA–LDA model in Table 1.

Table 1 Confusion table of the PCA–LDA classification model to discriminate HSCs and hepatocytes using their vibrational signatures. (A) Confusion table for the training data using lipid droplet spectra not containing retinol of 10 different HSCs and hepatocytes from two independent isolations. (B) Confusion table of the same PCA–LDA model with independent validation data using lipid droplet spectra not containing retinol of four different HSCs and hepatocytes from a third independent isolation

	HSC	Hepatocyte
A		
HSC (train batch)	250	0
Hepatocyte (train batch)	0	182
B		
HSC (test batch)	233	4
Hepatocyte (test batch)	0	281

a living tissue slice generated with the N-FINDR algorithm. Regions with similar spectral features are depicted in the same color and the corresponding averaged Raman spectra are shown in Fig. 7B. Spectra dominated by the retinol pattern can be found distributed over the slice and are a clear evidence for the presence of quiescent HSCs. In the surrounding, spectral characteristics at 748 cm^{-1} and 1589 cm^{-1}, which can be assigned to cytochrome vibrations, indicate the presence of hepatocytes. Raman spectroscopic detection of retinol in liver cryo-slices has been reported previously by Kochan *et al.*[54] However, the authors describe the retinol to be present only in rare cases, while it was found with minor effort in high amounts in our study. Compared to HSC autofluorescence images (Fig. 1B) the high retinol abundance is more likely to reflect reality as the retinol storing HSCs are spread over the liver. In contrast to Kochan *et al.*,[54] fresh precision-cut living slices were used in the presented study. It agrees with our own experience that retinol patterns are hard to identify in frozen liver tissue sections. Probably this is caused by sample processing and light sensitivity of retinol.

HSC identification in freshly sampled mouse liver

To pave the way for *in vivo* analyses fresh intact mouse liver was studied. The characteristic retinol pattern (Fig. 3B) was detected repeatedly in Raman maps of fresh intact mouse liver (Fig. 7C and D, d) sampled from healthy animals. From the N-FINDR false color Raman images a dimension of around 10 μm can be estimated for a quiescent HSC (Fig. 7C). Comparison with an immunofluorescence stained liver cryo-slice (Fig. 8) shows that this size corresponds well to the dimension of a HSC in tissue surrounding. Thus, retinol is confirmed to be a suitable native marker for Raman spectroscopy based non-destructive, tissue-preservative and label-free identification of quiescent stellate cells in the intact organ. The known disadvantage of fast signal bleaching observed during retinol autofluorescence detection was not encountered during Raman spectroscopic analysis.

Healthy, intact liver is expected to contain no or only very few activated stellate cells. In order to detect the characteristic Raman spectroscopic signature of activated HSCs in the tissue, Raman maps were recorded from an intact liver sample derived from a mouse treated with lipopolysaccharide (LPS) 24 h prior to organ sampling. LPS is known to cause an inflammatory

Downloaded from https://academic.oup.com/ib/article/6/10/946/5199050 by University of Alabama at Birmingham user on 27 May 2022

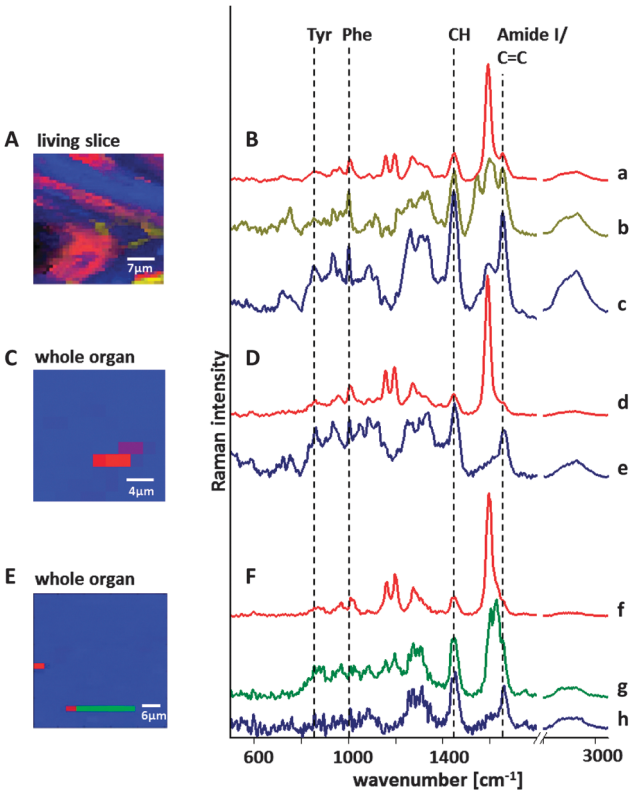

Fig. 7 Identification of HSCs in tissue. (A, C, E) False color N-FINDR Raman images of HSCs in an organ slice (A) and whole organs (C from healthy mouse and E from LPS treated mouse). (B, D, F) Average spectra are depicted according to N-FINDR unmixing. Colors correspond to colors used in the N-FINDR images (A, C, E). Quiescent HSCs are identified by retinol presence (red, spectra a, d, f). In the whole organ (E) Raman spectra of an activated HSC (green, spectrum g) were detected next to retinol spectra.

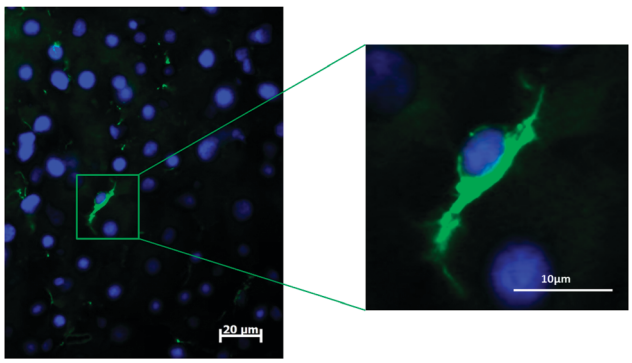

Fig. 8 HSC fluorescence image in tissue (independent 4 µm cryo-slice). GFAP-labeled HSCs (green) are visible surrounded by unstained hepatocytes and other non-parenchymal cells, nuclei are stained with DAPI (blue). One HSC is enlarged for improved HSC size and shape estimation.

response in the host as is also induced during acute sepsis and thus lead to acute organ injury.[47,55] Hence, presence of an increased number of activated HSCs is expectable and the vibrational spectroscopic signature identified in the *in vitro* culture-induced activation experiments (Fig. 3C) should be present. Fig. 7E shows a false color N-FINDR Raman image from a whole liver after LPS treatment; in Fig. 7F the corresponding average Raman spectra are displayed. The typical vibrational bands of retinol can be still detected (Fig. 7F, spectrum f). However, the close resemblance of the green spectrum (Fig. 7F, g) and the spectra belonging to an *in vitro* cultured HSC in its transforming state (Fig. 3C, spectrum l) clearly point to the presence of an HSC transforming from the quiescent to the activated state. This HSC (Fig. 7E) is situated in its natural environment. The close spatial vicinity of the retinol vibrational signature and the characteristic vibrational signature of lipid droplets in activated HSCs in the *in situ* acquired Raman map (Fig. 7E) indicates the presence of a HSC with a similar activation state as depicted in Fig. 2B, l. This proves that not only quiescent HSCs, but also activated HSCs are well delimitable against surrounding tissue parts using the specific Raman spectroscopic signatures. The knowledge of HSC vibrational lipid signatures occurring during the activation process allows for conclusions on their activation state in the complex tissue context.

Conclusion

Raman and immunofluorescence data derived from HSC *in vitro* studies in this contribution provide insights into the multifaceted activation process of hepatic stellate cells. The experimental data illustrate the tight link between retinol loss and the onset of HSC activation. Information on the HSC vibrational phenotype is gained and complements the already well documented molecular phenotype.[10,18,19] Furthermore, the *in vitro* data form the basis for HSC identification in tissue surroundings. Quiescent hepatic stellate cells exhibit a specific and very characteristic Raman signature due to their retinol content. This allows for easy identification of quiescent HSCs in early primary cell cultures as well as in tissue samples, such as living slices and whole intact livers. The position and shape of an HSC within complex tissue and intact organ can be visualized by Raman spectroscopic imaging in a label-free and non-destructive manner. Furthermore, Raman imaging using NIR excitation at moderate laser power and exposure time does not interfere with the cell's metabolism and does not destroy (bleach) the retinol. This marks an important advantage over established autofluorescence detection of HSCs using retinol as an intrinsic fluorophore.[20,56] In order to excite the retinol autofluorescence UV light is necessary. This high-energy excitation marks a serious disturbance for a living sample. It not only causes fast bleaching of the retinol fluorescence and thus a loss of this cell type marker, but the photochemical destruction of retinol also prevents proper integration of retinol in the physiological signaling pathway *via* conversion into retinoic acid.[57] Thus, retinol destruction by the probing process during cell type identification has to be prevented urgently. This is achieved with the presented Raman spectroscopic imaging technique.

Furthermore, vibrational spectroscopic characterization of HSCs is not limited to quiescent stellate cells. Characteristic vibrational signatures of the (retinol-free) lipid droplets of activated HSCs allow for a differentiation from surrounding hepatocytes as well

Downloaded from https://academic.oup.com/ib/article/6/10/946/5199050 by University of Alabama at Birmingham user on 27 May 2022

 This journal is © The Royal Society of Chemistry 2014

as the recognition of a HSC transforming from its quiescent to its activated state *in situ*. Generally, Raman spectroscopy is applicable *in vivo*.[58] Thus, the suitability of Raman spectroscopy to assess the HSC activation state *in vivo*, *e.g.*, as a tool to prove HSC response to vasoactive stimuli, paves the way for analyses of the role of HSCs in acute and chronic diseases.

Experimental

Chemicals

Retinyl palmitate (Sigma-Aldrich Chemie GmbH, Germany) was mixed 1 : 4 in isopropanol (Carl Roth GmbH & Co. KG, Germany) for the acquisition of the retinyl palmitate reference spectrum.

Animal samples

Female C57/B6 mice and female FVB/NJ mice were used in this study. Mice were allowed to adapt to laboratory conditions for at least 4 days. Animals were maintained under artificial day–night cycles (12 h light–dark cycles; 23 °C room temperature; 30–60% environment humidity) and received a standard mouse diet and water *ad libitum*. All investigations were performed in accordance with German legislation on protection of animals and with permission of the regional animal welfare committee of Thuringia.

Cell isolation, culture and fixation

Mouse HSCs from C57/B6 and FVB/NJ and hepatocytes from C57/B6 were isolated with a two-step collagenase-pronase digestion based on and modified from Maschmeyer *et al.*[59] Briefly, mice were anaesthetized with 2% isoflurane followed by an isolated liver perfusion *via* the portal vein. Liver was digested with 0.5 mg ml^{-1} pronase (Roche Pharma AG, Germany), followed by a 0.4 mg ml^{-1} collagenase (Roche Pharma AG, Germany) perfusion. Liver tissue was further detached while stirring in a combined pronase, collagenase and DNase (AppliChem GmbH, Germany) solution. Afterwards, cells were filtered through a 100 μm cell strainer and separated using Nycodenz (Axis-Shield plc, Norway) gradient centrifugation. Hepatocytes were pelleted at the bottom while HSCs were collected from the interphase of the gradient solution. HSCs for measurements at day 0 were pelleted after a washing step with PBS (Biochrom AG, Germany) and immediately fixed with 4% formalin (Rotifix, Carl Roth GmbH & Co. KG, Germany) at 4 °C for 10 min. The cells were pelleted again and resuspended in 0.75% alginate solution (Sigma-Aldrich Chemie GmbH, Germany). The alginate cell suspension was forced thereafter to polymerize on CaF_2 slides by addition of 0.5 M $CaCl_2$ solution. Cells for *in vitro* culture were seeded on CaF_2 slides in 24 well plates. Cells were cultured at 37 °C with 5% CO_2 atmosphere. Culture medium for HSCs was DMEM/F12 (Life Technologies GmbH, Germany) with 10% FCS (Biochrom AG, Berlin, Germany) and initially 1% penicillin/streptomycin (Life Technologies GmbH, Germany) until the first medium exchange 12 hours after isolation. Hepatocytes were cultivated in Williams E medium (Biochrom AG, Germany) containing 0.1 μM insulin (Sigma-Aldrich Chemie GmbH, Germany), 10% GlutaMaxx (Life Technologies GmbH, Germany), 50 μg ml^{-1} Gentamicin (Life Technologies GmbH, Germany) and 25 mM glucose (B. Braun Melsungen AG, Germany). Prior to Raman measurements, HSCs after different cultivation times (day 1, day 2, day 5, day 14) and hepatocytes (day 1 after isolation) for comparison were washed with PBS on the CaF_2 slides and fixed with Rotifix solution as described above.

Cells were derived from three independent isolations. HSC isolation from the two mice strains gave different HSC yields, but no Raman spectroscopic differences were found (data not shown). Fixed samples were maintained in PBS.

Generation of precision-cut living tissue slices

A C57/B6 mouse was sacrificed by isoflurane inhalation and its liver was sampled. The freshly isolated liver was kept in 4 °C Krebs–Henseleit buffer (Biochrom AG, Germany). A punch was obtained immediately and inserted into a Krumdieck tissue slicer (Alabama, USA). Thereafter, several slices of about 1 mm thickness were cut. Slices were instantly transferred onto CaF_2 slides and incubated in pre-oxygenized (30 min carbogen gas) Williams E culture medium containing the same additives as used for hepatocyte cell culture at 37 °C with 5% CO_2 atmosphere for at least 30 min prior to Raman measurements. Slices were used for Raman measurements no longer than 4 h after generation.

Sampling of intact mouse liver and LPS treatment

Two C57/B6 mice were sacrificed by cervical dislocalisation prior to liver sampling, one mouse received LPS treatment. In the LPS treated mouse, LPS (11 mg kg^{-1} body weight) was injected once intraperitoneal at the start of the experiment. No further treatment was administered. Animals were scored 24 h after the insult and the body weight was measured. The clinical severity score reflects spontaneous activity, the response to exogenous stimuli and posture.[60] Freshly sampled livers were transported in physiologic NaCl (Biochrom AG, Germany) solution. Raman spectra were acquired immediately upon arrival.

Raman spectra acquisition

A Raman spectrometer (alpha 300, Witec, Germany) equipped with a 785 nm diode laser (Toptica Photonics AG, Germany) and 532 nm frequency-doubled Nd:YAG laser (Witec, Germany) was used for all measurements. Laser light is coupled *via* fibers into an upright microscope (Carl Zeiss AG, Germany) and focused at the sample *via* an objective lens. A 60× water immersion objective with NA 1.0 (Nikon GmbH, Germany) was used for measurements in liquid, a 100× LD objective with NA 0.9 (Carl Zeiss AG, Germany) for dry measurements. 180° backscattered light was collected through the same optics and transferred *via* a fiber across a grating for wavelength splitting to the detector. In fixed samples (isolated cells) the 532 nm laser served for excitation applying 15 mW power to the sample. The scattered light was lead through a fiber with a diameter of 25 μm onto a 300 lines per mm grating before striking the back-illuminated CCD detector (DV401A-BV-352 cooled to −60 °C, ANDOR, Ireland). For living samples (tissue slice and whole organ),

Downloaded from https://academic.oup.com/ib/article/6/10/946/5199050 by University of Alabama at Birmingham user on 27 May 2022

the 785 nm laser with a power of 100 mW in the sample plane served for excitation, a fiber with 100 μm diameter lead the Raman scattered light onto a 600 lines per mm grating before arriving at the deep-depletion back-illuminated CCD detector (DU401A-BR-DD-352, cooled to −60 °C, ANDOR, Ireland).

Spectra were acquired in mapping mode with an integration time of 1 s per spectrum. Step size between single spectra ranged from 0.5 μm in fixed single cells to 1–2 μm in living samples.

For each fixation time point, maps of at least seven different cells or parts of them were obtained.

Chemically fixed samples were measured in PBS at ambient temperature, living slices in their culture medium at 37 °C. Stable incubation temperature was guaranteed by an in house built heating device with integrated temperature sensor. Intact liver was kept moist with physiologic NaCl solution and measured at ambient temperature with a long distance dry objective to avoid leachate of fluorescent molecules and the along coming fluorescence background.

Analysis of Raman data

Matlab (MathWorks, Germany) and GNU R[61] served for spectra pretreatment and processing. Cosmic spikes were removed employing the cosmic ray removal function in Matlab.

Image analysis was done with Matlab algorithms. Spectra were cut to the wavenumber region from 350 to 3050 cm^{-1}. Principal component analysis (PCA)[62] served for noise reduction: only the first 10 PCs describing more than 99% of the whole variance were kept. To process single cell Raman maps, hierarchical cluster analysis (HCA)[62] was used to distinguish cell spectra from background spectra. The latter were excluded from further analysis. As the final unmixing algorithm N-FINDR analysis[62] was performed taking into account the wavenumber region from 600 to 1800 cm^{-1} and including extended multiplicative signal correction (EMSC)-based[63] spectra normalization. The expectation of two to three endmembers depending on the dataset was used as input value.

The cell type classification with PCA and PCA–linear discriminant analysis (PCA-LDA) was carried out in R using pretreated Raman spectra with truncated wavenumber axis and without spikes (from Matlab). Relevant spectra were concluded from the distance of the respective spectrum to a certain endmember according to N-FINDR. For PCA/PCA–LDA with lipid droplet spectra the endmember of interest had to contribute with at least 75%. For PCA with nuclei derived spectra the endmember of interest had to contribute with at least 80%. In R data were processed exclusively in the hyperSpec environment.[64] Baselines were calculated relying on a second order polynomial and subtracted. The wavenumber axis was further cut to the region from 600 to 1800 cm^{-1} and vector normalization was done. To build the lipid droplet PCA–LDA model the first 5 PCs were kept describing 95% of the variance. Together 432 spectra of HSCs and hepatocytes from two independent isolations were included. With respect to HSCs spectra of cells cultured for 0, 1, 5 and 14 days were considered. A number of 518 spectra derived from cells of a third independent isolation were used to test the classification model.

Average spectra for compartments were calculated from those spectra that consisted of a N-FINDR endmember of interest to at least 75%. Spectra from the N-FINDR analysis shown in the figures were plotted in Origin (Origin Lab Corporation, MA, USA) and received polynomial baseline subtraction. Up to eight anchorage points were set manually.

Estimation of the cellular retinol content from the Raman data

The quotient of the sum of retinol positive spectra and the sum of all cell spectra was calculated for HSCs measured between day 0 and day 5 after isolation. A spectrum was counted as retinol positive if the N-FINDR retinol endmember contributed with at least 75%. A boxplot was derived from those quotients running Matlab function 'boxplot'.

Immunofluorescence labeling and fluorescence image acquisition

Fixed samples were immunofluorescence-labeled after the Raman measurements. The labeling procedure included antigen retrieval with Tris/EDTA solution (Carl Roth GmbH & Co. KG, Germany) at 95 °C, cell membrane permeabilization with Tween-20 (Carl Roth GmbH & Co. KG, Germany) and a blocking step with blocking reagent (Life Technologies GmbH, Germany). This was followed by two step labeling either against one antigen (E-Cadherin) only or in a consecutive way against GFAP and ASMA as the antigens in a double-labeling process. A polyclonal chicken-anti-E-Cadherin antibody (Abcam plc, UK) served as the primary antibody against E-Cadherin. The secondary antibody carrying the fluorophore was a polyclonal donkey-anti-chicken-Cy3 (Dianova GmbH, Germany). The primary antibody against GFAP was a monoclonal mouse-anti-GFAP antibody (New England Biolabs GmbH, Germany) that was detected by a polyclonal donkey-anti-mouse-Cy3 secondary antibody (Dianova GmbH, Germany). As the primary antibody against ASMA a polyclonal rabbit-anti-ASMA antibody (Abcam plc, UK) was used and combined with a polyclonal goat-anti-rabbit-Alexa488 secondary antibody (Dianova GmbH, Germany) for detection. After labeling the samples were embedded with Vectashield containing DAPI as additive (Linaris GmbH, Germany).

In tissue cryo-slices GFAP was labeled first with a rabbit-anti-GFAP monoclonal antibody (Abcam plc, UK) and detected using a goat-anti-rabbit-Alexa488 polyclonal antibody (Dianova GmbH, Germany). Tissue samples were fixed with −20 °C acetone, no antigen retrieval was done.

Immunofluorescence and auto-fluorescence images were acquired with an upright *epi*-fluorescence microscope (Axioplan 2, Carl Zeiss AG, Germany) equipped with a HBO 50/AC light source for fluorescence excitation, an AxioCam HRc camera (Carl Zeiss AG, Germany) served as the detector of fluorescence emission. The excitation filters, beam splitters and emission filters were as follows: for Alexa488: BP 450–490, FT 510, LP 515, for Cy3: BP 560/40, FT 585, BP 630/75, for DAPI and retinol autofluorescence: BP 365/12, FT 395, LP 397 (all from Carl Zeiss AG, Germany). Image acquisition was done with Zeiss Axio Vert software (Carl Zeiss AG, Germany).

Downloaded from https://academic.oup.com/ib/article/6/10/946/5199050 by University of Alabama at Birmingham user on 27 May 2022

 This journal is © The Royal Society of Chemistry 2014

Acknowledgements

Financial support by the DFG *via* the research group FOR 1738 ''Heme and heme degradation products'' and the BMBF (FKZ 01EO1002, Integrated Research and Treatment Center ''Center for Sepsis Control and Care'') is highly acknowledged.

References

1 A. Geerts, *Semin. Liver Dis.*, 2001, **21**, 311–335.
2 F. Winau, G. Hegasy, R. Weiskirchen, S. Weber, C. Cassan, P. A. Sieling, R. L. Modlin, R. S. Liblau, A. M. Gressner and S. H. Kaufmann, *Immunity*, 2007, **26**, 117–129.
3 H. Rensing, I. Bauer, J. X. Zhang, M. Paxian, B. Pannen, Y. Yokoyama, M. G. Clemens and M. Bauer, *Hepatology*, 2002, **36**, 1453–1465.
4 H. Reynaert, D. Urbain and A. Geerts, *Anat. Rec.*, 2008, **291**, 693–698.
5 R. Bataller and D. A. Brenner, *J. Clin. Invest.*, 2005, **115**, 209–218.
6 Y. S. Lee and W. I. Jeong, *J. Gastroenterol. Hepatol.*, 2012, **27**(suppl 2), 75–79.
7 C. Coulouarn, A. Corlu, D. Glaise, I. Guenon, S. S. Thorgeirsson and B. Clement, *Cancer Res.*, 2012, **72**, 2533–2542.
8 D. Y. Zhang and S. L. Friedman, *Hepatology*, 2012, **56**, 769–775.
9 R. Salguero Palacios, M. Roderfeld, S. Hemmann, T. Rath, S. Atanasova, A. Tschuschner, O. A. Gressner, R. Weiskirchen, J. Graf and E. Roeb, *Lab. Invest.*, 2008, **88**, 1192–1203.
10 P. Sancho-Bru, R. Bataller, X. Gasull, J. Colmenero, V. Khurdayan, A. Gual, J. M. Nicolas, V. Arroyo and P. Gines, *J. Hepatol.*, 2005, **43**, 272–282.
11 M. Abdalla, A. Goc, L. Segar and P. R. Somanath, *J. Biol. Chem.*, 2013, **288**, 33483–33493.
12 M. Franz, K. Grun, P. Richter, B. R. Brehm, M. Fritzenwanger, K. Hekmat, D. Neri, J. Gummert, H. R. Figulla, H. Kosmehl, A. Berndt and A. Renner, *Histochem. Cell Biol.*, 2010, **134**, 503–517.
13 B. Hinz, G. Celetta, J. J. Tomasek, G. Gabbiani and C. Chaponnier, *Mol. Biol. Cell*, 2001, **12**, 2730–2741.
14 W. S. Blaner, S. M. O'Byrne, N. Wongsiriroj, J. Kluwe, D. M. D'Ambrosio, H. Jiang, R. F. Schwabe, E. M. Hillman, R. Piantedosi and J. Libien, *Biochim. Biophys. Acta*, 2009, **1791**, 467–473.
15 S. L. Friedman, *Semin. Liver Dis.*, 1999, **19**, 129–140.
16 D. N. D'Ambrosio, J. L. Walewski, R. D. Clugston, P. D. Berk, R. A. Rippe and W. S. Blaner, *PLoS One*, 2011, **6**, e24993.
17 A. B. Cubitt, R. Heim, S. R. Adams, A. E. Boyd, L. A. Gross and R. Y. Tsien, *Trends Biochem. Sci.*, 1995, **20**, 448–455.
18 J. Ji, F. Yu, Q. Ji, Z. Li, K. Wang, J. Zhang, J. Lu, L. Chen, Q. E, Y. Zeng and Y. Ji, *Hepatology*, 2012, **56**, 332–349.
19 F. Jiang, C. J. Parsons and B. Stefanovic, *J. Hepatol.*, 2006, **45**, 401–409.
20 K. Hellemans, K. Rombouts, E. Quartier, A. S. Dittie, A. Knorr, L. Michalik, V. Rogiers, F. Schuit, W. Wahli and A. Geerts, *J. Lipid Res.*, 2003, **44**, 280–295.
21 Y. Kida, Z. Xia, S. Zheng, N. M. Mordwinkin, S. G. Louie, S. G. Zheng, M. Feng, H. Shi, Z. Duan and Y. P. Han, *PLoS One*, 2011, **6**, e26644.
22 T. F. Lee, K. M. Mak, O. Rackovsky, Y. L. Lin, A. J. Kwong, J. C. Loke and S. L. Friedman, *J. Cell. Physiol.*, 2010, **223**, 648–657.
23 H. Moriwaki, W. S. Blaner, R. Piantedosi and D. S. Goodman, *J. Lipid Res.*, 1988, **29**, 1523–1534.
24 S. M. O'Byrne, N. Wongsiriroj, J. Libien, S. Vogel, I. J. Goldberg, W. Baehr, K. Palczewski and W. S. Blaner, *J. Biol. Chem.*, 2005, **280**, 35647–35657.
25 F. Bonnier, S. M. Ali, P. Knief, H. Lambkin, K. Flynn, V. McDonagh, C. Healy, T. C. Lee, F. M. Lyng and H. J. Byrne, *Vib. Spectrosc.*, 2012, **61**, 124–132.
26 G. J. Puppels, J. H. F. Olminkhof, G. M. J. Segersnolten, C. Otto, F. F. M. Demul and J. Greve, *Exp. Cell Res.*, 1991, **195**, 361–367.
27 K. Galler, K. Brautigam, C. Grosse, J. Popp and U. Neugebauer, *Analyst*, 2014, **139**, 1237–1273.
28 C. Krafft, B. Dietzek and J. Popp, *Analyst*, 2009, **134**, 1046–1057.
29 G. J. Puppels, F. F. de Mul, C. Otto, J. Greve, M. Robert-Nicoud, D. J. Arndt-Jovin and T. M. Jovin, *Nature*, 1990, **347**, 301–303.
30 U. Neugebauer, T. Bocklitz, J. H. Clement, C. Krafft and J. Popp, *Analyst*, 2010, **135**, 3178–3182.
31 A. Taleb, J. Diamond, J. J. McGarvey, J. R. Beattie, C. Toland and P. W. Hamilton, *J. Phys. Chem. B*, 2006, **110**, 19625–19631.
32 A. Ramoji, U. Neugebauer, T. Bocklitz, M. Foerster, M. Kiehntopf, M. Bauer and J. Popp, *Anal. Chem.*, 2012, **84**, 5335–5342.
33 K. Hartmann, M. Becker-Putsche, T. Bocklitz, K. Pachmann, A. Niendorf, P. Rosch and J. Popp, *Anal. Bioanal. Chem.*, 2012, **403**, 745–753.
34 C. Krafft, B. Belay, N. Bergner, B. F. Romeike, R. Reichart, R. Kalff and J. Popp, *Analyst*, 2012, **137**, 5533–5537.
35 T. Meyer, N. Bergner, A. Medyukhina, B. Dietzek, C. Krafft, B. F. Romeike, R. Reichart, R. Kalff and J. Popp, *J. Biophotonics*, 2012, **5**, 729–733.
36 P. Matousek and N. Stone, *J. Biophotonics*, 2013, **6**, 7–19.
37 C. Krafft, T. Knetschke, R. H. Funk and R. Salzer, *Anal. Chem.*, 2006, **78**, 4424–4429.
38 M. Okada, N. I. Smith, A. F. Palonpon, H. Endo, S. Kawata, M. Sodeoka and K. Fujita, *Proc. Natl. Acad. Sci. U. S. A.*, 2012, **109**, 28–32.
39 M. Pudlas, E. Brauchle, T. J. Klein, D. W. Hutmacher and K. Schenke-Layland, *J. Biophotonics*, 2013, **6**, 205–211.
40 I. W. Schie, J. Wu, T. Weeks, M. A. Zern, J. C. Rutledge and T. Huser, *J. Biophotonics*, 2011, **4**, 425–434.
41 N. Testerink, M. Ajat, M. Houweling, J. F. Brouwers, V. V. Pully, H. J. van Manen, C. Otto, J. B. Helms and A. B. Vaandrager, *PLoS One*, 2012, **7**, e34945.
42 G. Buniatian, B. Hamprecht and R. Gebhardt, *Biol. Cell*, 1996, **87**, 65–73.
43 J. W. Chan, D. Motton, J. C. Rutledge, N. L. Keim and T. Huser, *Anal. Chem.*, 2005, **77**, 5870–5876.

Downloaded from https://academic.oup.com/ib/article/6/10/946/5199050 by University of Alabama at Birmingham user on 27 May 2022

44 C. Krafft, T. Knetschke, A. Siegner, R. H. W. Funk and R. Salzer, *Vib. Spectrosc.*, 2003, **32**, 75–83.

45 N. Failloux, I. Bonnet, M. H. Baron and E. Perrier, *J. Appl. Spectrosc.*, 2003, **57**, 1117–1122.

46 L. Xu, A. Y. Hui, E. Albanis, M. J. Arthur, S. M. O'Byrne, W. S. Blaner, P. Mukherjee, S. L. Friedman and F. J. Eng, *Gut*, 2005, **54**, 142–151.

47 Z. Kmiec, *Adv. Anat., Embryol. Cell Biol.*, 2001, **161**(III–XIII), 1–151.

48 J. E. Davies, P. Hodge, F. D. Gunstone and M. S. Lie Ken Jie, *Chem. Phys. Lipids*, 1975, **15**, 48–52.

49 K. Fujita and N. I. Smith, *Mol. Cells*, 2008, **26**, 530–535.

50 M. Ogawa, Y. Harada, Y. Yamaoka, K. Fujita, H. Yaku and T. Takamatsu, *Biochem. Biophys. Res. Commun.*, 2009, **382**, 370–374.

51 O. Pelkonen, M. Turpeinen, J. Hakkola, P. Honkakoski, J. Hukkanen and H. Raunio, *Arch. Toxicol.*, 2008, **82**, 667–715.

52 A. J. Gandolfi, J. Wijeweera and K. Brendel, *Toxicol. Pathol.*, 1996, **24**, 58–61.

53 S. Thohan, M. C. Zurich, H. Chung, M. Weiner, A. S. Kane and G. M. Rosen, *Drug Metab. Dispos.*, 2001, **29**, 1337–1342.

54 K. Kochan, K. M. Marzec, K. Chruszcz-Lipska, A. Jasztal, E. Maslak, H. Musiolik, S. Chlopicki and M. Baranska, *Analyst*, 2013, **138**, 3885–3890.

55 M. Dirlik, A. Karahan, H. Canbaz, M. Caglikulekci, A. Polat, L. Tamer and S. Aydin, *Curr. Ther. Res.*, 2009, **70**, 299–315.

56 H. Popper, *Phys. Rev.*, 1944, **24**, 205–224.

57 G. Shiota and K. Kanki, *J. Gastroenterol. Hepatol.*, 2013, **28**(suppl 1), 33–37.

58 S. E. Bohndiek, A. Wagadarikar, C. L. Zavaleta, D. Van de Sompel, E. Garai, J. V. Jokerst, S. Yazdanfar and S. S. Gambhir, *Proc. Natl. Acad. Sci. U. S. A.*, 2013, **110**, 12408–12413.

59 P. Maschmeyer, M. Flach and F. Winau, *J. Visualized Exp.*, 2011, **51**, DOI: 10.3791/2710.

60 F. A. Gonnert, P. Recknagel, M. Seidel, N. Jbeily, K. Dahlke, C. L. Bockmeyer, J. Winning, W. Losche, R. A. Claus and M. Bauer, *J. Surg. Res.*, 2011, **170**, e123–e134.

61 R. Development Core Team, R Foundation for Statistical Computing, R version 2.15.3 (2013-03-01) edn, Vienna, Austria, 2013.

62 M. Hedegaard, C. Matthaus, S. Hassing, C. Krafft, M. Diem and J. Popp, *Theor. Chem. Acc.*, 2011, **130**, 1249–1260.

63 N. K. Afseth and A. Kohler, *Chemom. Intell. Lab. Syst.*, 2012, **117**, 92–99.

64 C. Beleites and V. Sergo, http://hyperspec.r-forge.r-project.org, package version 0.98-20120923 edn.

Downloaded from https://academic.oup.com/ib/article/6/10/946/5199050 by University of Alabama at Birmingham user on 27 May 2022

 This journal is © The Royal Society of Chemistry 2014